Available online at www.sciencedirect.com

SciVerse ScienceDirect

Ceramics International 38 (2012) 4607–4615

CERAMICS INTERNATIONAL

www.elsevier.com/locate/ceramint

Effect of various additives on morphology and corrosion behavior of ceramic coatings developed on AZ31 magnesium alloy by plasma electrolytic oxidation

D. Sreekanth, N. Rameshbabu *, K. Venkateswarlu

Department of Metallurgical and Materials Engineering, National Institute of Technology, Tiruchirappalli 620015, Tamilnadu, India

Received 29 December 2011; received in revised form 10 February 2012; accepted 10 February 2012
Available online 21 February 2012

Abstract

Plasma electrolytic oxidation (PEO) coatings were developed on AZ31 magnesium alloy using alkaline silicate with KOH as a base electrolyte system, and with the addition of sodium aluminate, sodium tetra borate, potassium titanium fluoride, tri sodium ortho phosphate and urea as additives. The phase composition and surface morphology of these multi-phase coatings were analyzed by X-ray diffraction (XRD) and scanning electron microscopy (SEM). The corrosion behavior of the coated samples was evaluated by potentiodynamic polarization tests and electrochemical impedance spectroscopy (EIS) in 3.5 wt.% NaCl solution. The results showed that the anions namely, SiO_3^{2-}, AlO_2^-, $B_4O_7^{2-}$, F^- and PO_4^{3-}, effectively participated in the coating formation influencing its chemical composition and surface morphology and thereby corrosion resistance. The mechanism of corrosion process of each coating was explained in detail with the help of Electrochemical Impedance Spectroscopy (EIS) analysis and equivalent circuit modeling. It was observed that the sample treated by PEO in the electrolyte solution containing sodium tetra borate as an additive showed higher corrosion resistance which could be attributed to its morphological characteristics.

Keywords: A. Films; B. Porosity; C. Corrosion; E. Structural applications

1. Introduction

Plasma electrolytic oxidation (PEO) is an emerging environment friendly technology for the production of corrosion and wear resistant coatings on light metals such as aluminium, magnesium, titanium and zirconium [1–4]. This method is based on the anodic polarization of a metal in an aqueous solution of an electrolyte at voltages that cause the occurrence of plasma micro discharges at the electrode surface. This leads to the dissolution of metal ions, which in turn react with anions from the electrolyte, thereby forming respective metal oxides. The high temperature and pressure in breakdown channels create conducive conditions for the formation of these oxide structures [5]. Further, the inclusion of additives in the electrolyte leads to the formation of layers that consist of both oxides of the substrate as well as electrolyte specific phases which improve various properties of the coating such as corrosion resistance and wear resistance [6–10].

Magnesium and its alloys have been the focus of recent research for structural and biomedical implant applications owing to their high strength to weight ratio [11,12]. However, these alloys have low corrosion resistance due to their high chemical reactivity and lack of protective passive oxide film [13]. Surface modification processes such as PEO which enhance the corrosion resistance are being extensively studied in present day investigations. The corrosion resistance of coatings developed by PEO mainly depends on their composition and morphology [14,15]. In general, PEO coatings on Mg were found to be mainly composed of magnesium oxide along with other electrolyte-borne phases such as Mg_2SiO_4, $Mg_3(PO_4)_2$ or $MgAl_2O_4$, etc. [16–18]. These phases can be produced in the coating in two ways, either by using the respective compounds themselves as base electrolytes or by adding them as additives to any other base electrolyte. The main advantage of addition of small amounts of these compounds to

* Corresponding author. Tel.: +91 431 2503464; fax: +91 431 2500133.
E-mail addresses: nrb@nitt.edu, rameshrohith@gmail.com (N. Rameshbabu).

0272-8842/$36.00
doi:10.1016/j.ceramint.2012.02.040

the base electrolyte is the ability to produce multiple phases in the coating in a single step. Each of these phases has a particular property with respect to coating growth kinetics, adherence and chemical stability. By studying the corrosion mechanisms of such multi-phase coatings, the effect of various additives on the corrosion characteristics may be determined. Consequently, the optimum number and amount of additives to achieve the desired coating properties can be tailored.

The present research is focused on studying the role of various additives in modifying the phase structure, surface morphology and corrosion mechanism of PEO treated AZ31 magnesium alloy. The corrosion mechanism of each multi-phase coating is described by analyzing their electrochemical impedance data and modeling respective equivalent circuits.

2. Experimental

2.1. Preparation of sample

Rectangular coupons of AZ31 magnesium alloy of dimensions 25 mm × 15 mm × 2.5 mm were used as substrate material. Surface of all the samples were ground from 800 to 1200 grit SiC paper to ensure uniform surface roughness and subsequently cleaned ultrasonically with acetone and rinsed with distilled water to avoid any surface contamination prior to the PEO coating process. In order to ensure proper electrical contact, a threaded hole of 2 mm diameter was made on the edge of the sample and a thin aluminium rod which has external threading was screwed to the sample.

2.2. Preparation of electrolyte

The base electrolytic solution was prepared by adding 10 g/L of $Na_2SiO_3{\cdot}9H_2O$ and 4 g/L of KOH to 1 L of distilled water. Additives, namely, sodium aluminate, sodium tetra borate, potassium titanium fluoride, tri sodium ortho phosphate and urea, each 2 g/L, were added to base electrolyte solution and six different compositions of electrolyte were prepared. Table 1 lists these six electrolyte systems including the base electrolyte system, and the corresponding identification codes of the samples treated in these electrolytes. It may be noted that throughout the manuscript the coatings obtained by PEO in these electrolyte systems are identified by their respective codes.

Table 1
Sample codes and their respective electrolyte compositions of PEO treated AZ31 Mg alloy in different electrolyte systems.

Sample code	Composition of electrolyte
si-coat	10 g/L $Na_2SiO_3{\cdot}9H_2O$ + 4 g/L KOH
a-coat	10 g/L $Na_2SiO_3{\cdot}9H_2O$ + 4 g/L KOH + 2 g/L $NaAlO_2$
b-coat	10 g/L $Na_2SiO_3{\cdot}9H_2O$ + 4 g/L KOH + 2 g/L $Na_2B_4O_7.10H_2O$
k-coat	10 g/L $Na_2SiO_3{\cdot}9H_2O$ + 4 g/L KOH + 2 g/L K_2TiF_6
p-coat	10 g/L $Na_2SiO_3{\cdot}9H_2O$ + 4 g/L KOH + 2 g/L $Na_3PO_4.12H_2O$
u-coat	10 g/L $Na_2SiO_3{\cdot}9H_2O$ + 4 g/L KOH + 2 g/L CH_4N_2O

2.3. Fabrication of coating

The AZ31 Mg alloy samples prepared for PEO treatment were connected to the positive terminal of the power source, whereas the negative terminal was connected to the stainless steel bath containing electrolyte solution. During the PEO process, the electrolyte solution was stirred constantly using a magnetic stirrer to ensure proper dissipation of heat from the electrolyte. An indigenously designed pulsed DC power supply was employed for PEO treatment, which was capable of delivering voltage up to 650 V and current up to 15 A, with variable frequency and duty cycles. All the samples under study were treated in different electrolyte systems separately as listed in Table 1. Based on experimental trials, the parameters were fixed under constant current mode as current density of 60 mA/cm^2, frequency of 50 Hz, duty cycle of 50% and treatment time of 10 min.

2.4. Characterization of coating

Scanning electron microscope (S3000H, Hitachi, Japan) was employed to study the surface morphology and coating thickness of the PEO coated samples. The digitally stored images thus obtained were further processed using ImageJ image processing and analysis software for the quantification of pore characteristics (average area of pores and percentage area of porosity) and measurement of coating thickness. These measurements were carried out on surface and cross sectional SEM images of PEO treated samples taken at 4 different locations and their average values were calculated.

The phases formed in the PEO coatings were analyzed by using the X-ray diffractometer (UltimaIII, Rigaku, Japan) with Cu Kα radiation (λ = 0.154056 nm) at 40 kV and 30 mA with a scan speed of 1°/min and a step size of 0.05° over the 2θ range of 20° to 80°.

To evaluate the corrosion resistance of PEO coatings, potentiodynamic polarization tests and electrochemical impedance spectroscopy (EIS) were performed for the substrate and PEO treated samples using ACM Gill AC potentiostat (ACM Instruments, Cumbria, UK) with ACM's software package, which enabled the scan to be generated automatically under computer control. All polarization and EIS tests were carried out in 3.5 wt.% NaCl solution with a pH of 6.5. The corrosion cell consisted of a saturated calomel electrode (SCE) and a platinum foil, as reference and counter electrodes, respectively. Untreated and PEO treated Mg samples were used as working electrodes, exposing 0.5 cm^2 of area to the solution during electrochemical measurements. After an initial delay of 30 min, the polarization scan was conducted with a sweep rate of 100 mV/min and a start potential of −2000 mV up to a reversing potential of 2500 mV. EIS measurements were made from a start frequency of 10^5 Hz up to 0.01 Hz with AC signal amplitude of 10 mV RMS. After the measurements were obtained, the impedance data was analyzed by curve fitting and equivalent circuit modeling using ZView® software.

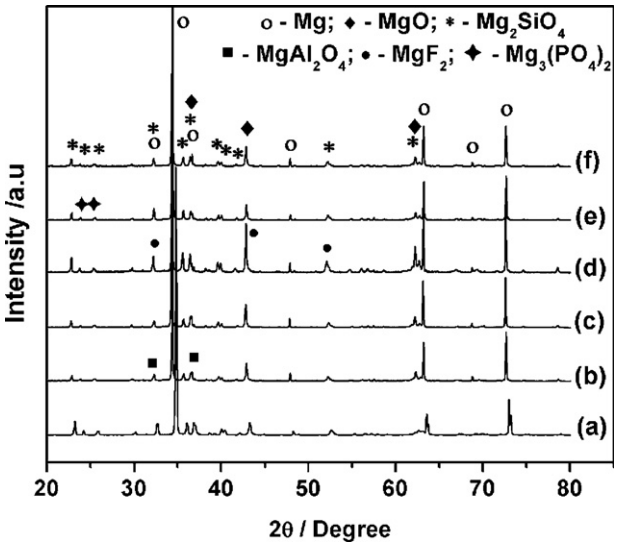

Fig. 1. XRD patterns of (a) si-coat, (b) a-coat, (c) b-coat, (d) k-coat, (e) p-coat and (f) u-coat.

3. Results and discussion

3.1. Phase analysis

XRD patterns of PEO coatings are shown in Fig. 1. In addition to the peaks corresponding to the substrate, all the patterns reveal the existence of MgO phase which is commonly found in PEO treated Mg alloys. Apart from MgO phase, these samples also contain Mg_2SiO_4 phase which corresponds to the reaction between the SiO_3^{2-} ions from $Na_2SiO_3.9H_2O$ present in the electrolyte system and Mg^{2+} ions from the substrate. The XRD results also show that the anions from the electrolyte additives effectively participate in the reaction and form respective electrolyte specific phases, such as $MgAl_2O_4$ in a-coat, MgF_2 in k-coat and $Mg_3(PO_4)_2$ in p-coat. The sharpness of all the diffraction peaks suggests that the fabricated coatings are crystalline in nature. The formation of different phases can be explained from the following reactions [10,19]:

$$Mg^{2+} + 2OH^- \rightarrow Mg(OH)_2 \rightarrow MgO + H_2O \quad (\text{at} \approx 332\,^{\circ}C) \tag{1}$$

$$2Mg^{2+} + SiO_3^{2-} + 2OH^- \rightarrow Mg_2SiO_4 + H_2O \tag{2}$$

$$Mg^{2+} + 2AlO_2^- \rightarrow Mg_2Al_2O_4 \tag{3}$$

$$Mg^{2+} + 2F^- \rightarrow MgF_2 \tag{4}$$

$$3Mg^{2+} + 2PO_4^{3-} \rightarrow Mg_3(PO_4)_2 \tag{5}$$

3.2. Morphology and cross section of coatings

Figs. 2 and 3 show the morphological and cross sectional features respectively, of all the PEO coatings obtained from electrolyte solutions containing different additives. It can be observed that the morphology of each coating is different from the other and all the coatings exhibit different levels of porosity. Since the shape of any pore is not perfectly circular, calculation of area of pore rather than the diameter of pore was considered to be appropriate. Therefore, in this study, the average size of pores and percentage area of porosity were considered in the analysis of pores. The numerical values of average pore size, percentage area of porosity and thickness of the coating measured by ImageJ software are summarized in Table 2. Although the obtained values may not be precise, they are useful in understanding the differences in the porosity characteristics among the coatings.

It can be noted by observing the surface morphologies of all the coatings (Fig. 2) and corresponding analysis of pores (Table 2) that there is a considerable difference in the levels of porosity among different samples coated in various electrolyte systems. Larger average pore size and higher percentage area of porosity

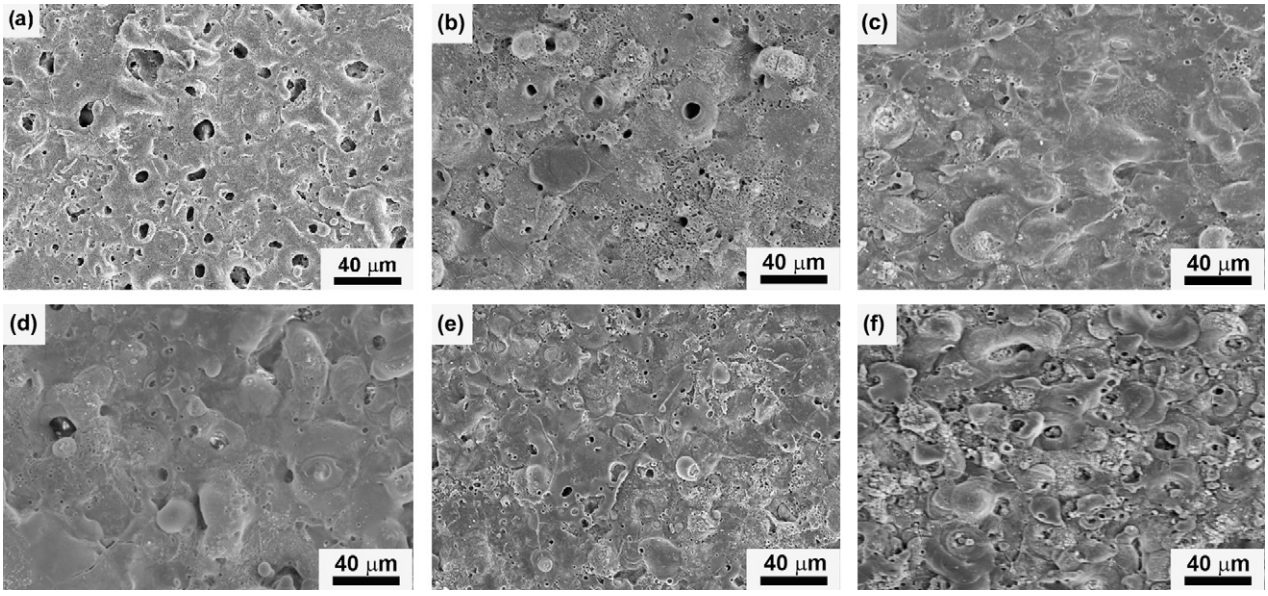

Fig. 2. SEM micrographs showing surface morphologies of (a) si-coat, (b) a-coat, (c) b-coat, (d) k-coat, (e) p-coat and (f) u-coat.

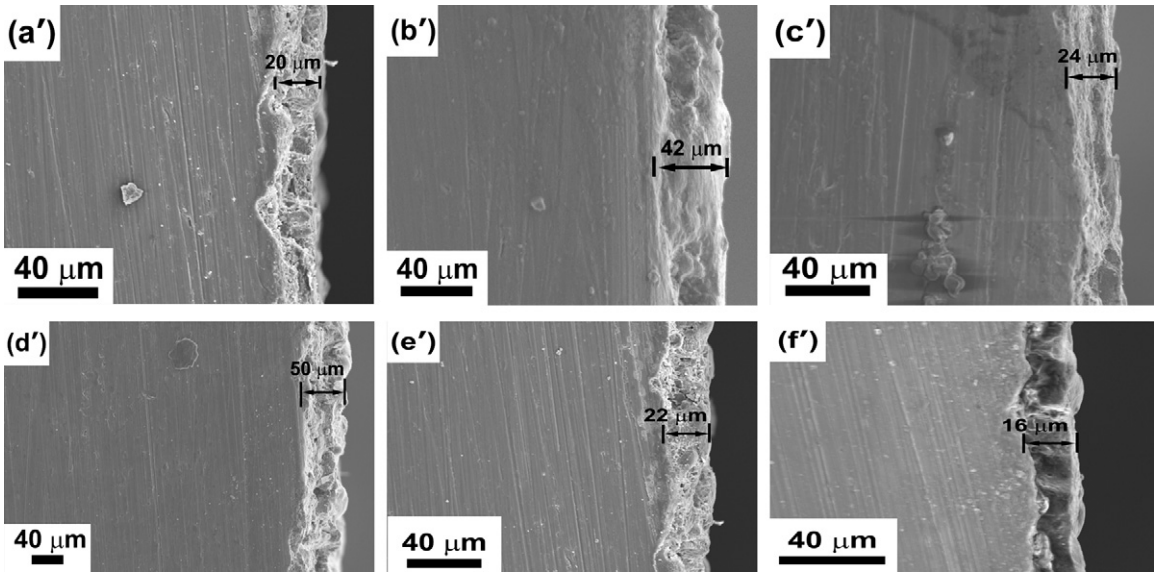

Fig. 3. SEM micrographs showing cross-sections of (a′) si-coat, (b′) a-coat, (c′) b-coat, (d′) k-coat, (e′) p-coat and (f′) u-coat.

was observed for si-coat, in contrast to b-coat which had the lowest values. The large variation in average size of pore and corresponding percentage area of porosity demonstrates that the addition of additives to the base electrolyte has significant influence on pore morphology. Further, it is evident from Table 2 that the coating thickness is largely influenced by anions in the electrolyte system. As compared to the thickness of si-coat obtained from base electrolyte solution, k-coat and a-coat show significant increase in the coating thickness. This can be attributed to F^- and AlO_2^- ions in the respective electrolytes which foster the growth rate of PEO coatings [20,21]. In case of the remaining coatings, there is no significant variation in the values of coating thickness implying that the anions such as $B_4O_7^{2-}$ and PO_4^{3-} do not have much influence on the coating thickness.

3.3. Potentiodynamic polarization study

The potentiodynamic polarization curves obtained for different PEO coatings in 3.5 wt.% NaCl solution is shown in Fig. 4. Corrosion potential (E_{corr}), corrosion current density (i_{corr}), and anodic/cathodic Tafel constant (β_a and β_c) were derived from these data by Tafel extrapolation method and are summarized in Table 3. The polarization resistance (R_p) was calculated using Stern–Geary equation [22]:

$$R_p = \frac{\beta_a \times \beta_c}{2.303 i_{corr}(\beta_a + \beta_c)} \quad (6)$$

The substrate, when exposed to corrosive NaCl medium, quickly forms a loose and porous $Mg(OH)_2$ layer. Increase in anodic potential leads to acceleration of Cl^- ions from the NaCl solution through this porous layer of $Mg(OH)_2$ and promotes dissolution of substrate. On the other hand, in case of PEO treated samples, the multi-phase oxide structure serves as a barrier to the transportation of corrosive ions and prevents their direct contact with the substrate. Therefore, in contrast with bare magnesium alloy AZ31, the samples treated in base silicate solution as well as with additives had more positive corrosion potential, greater negative corrosion current density

Table 2
Data of pore analysis and coating thickness of PEO treated AZ31 Mg alloy in different electrolyte systems.

Coating	Average size of pore/μm^2	Percentage area of porosity/%	Thickness of the coating/μm
si-coat	22.94	4.8	20
a-coat	10.85	2.8	42
b-coat	5.64	1.1	24
k-coat	7.4	2.3	50
p-coat	9.6	3.6	22
u-coat	7.97	2.6	16

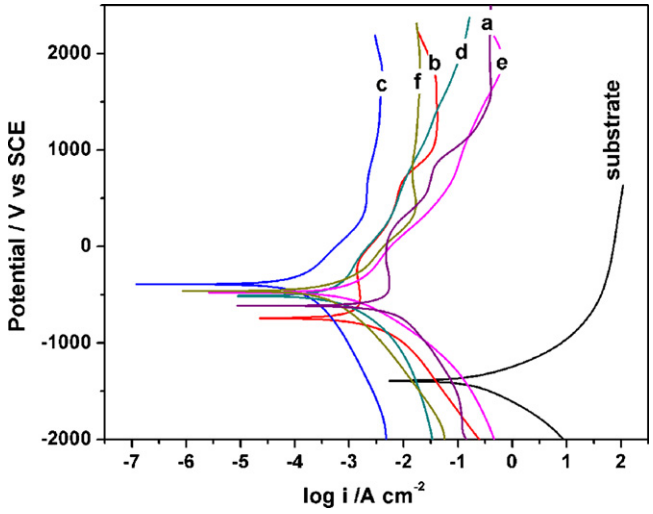

Fig. 4. Potentiodynamic polarization curves of substrate and PEO treated AZ31 Mg alloy in different electrolyte systems.

Table 3
Potentiodynamic polarization data of substrate and PEO treated AZ31 Mg alloy in different electrolyte systems.

Sample	β_a/mV	β_c/mV	E_{corr}/mV	i_{corr}/mA cm^{-2})	R_p/Ω cm^2
si-coat	709.23	263.64	−1521.6	3.21×10^{-3}	2.61×10^{1}
a-coat	674.48	210.42	−769.7	1.22×10^{-3}	5.46×10^{1}
b-coat	360.60	541.18	−377.8	1.01×10^{-4}	9.27×10^{2}
k-coat	622.30	270.82	−562.6	4.64×10^{-4}	1.78×10^{2}
p-coat	528.99	371.99	−486.1	1.03×10^{-3}	9.20×10^{1}
u-coat	322.81	679.01	−412.4	5.41×10^{-4}	1.77×10^{2}
Substrate	307.26	464.46	−1377.2	3.95×10^{-1}	3.95×10^{-4}

and higher polarization resistance. Among all the coatings obtained in different electrolyte systems, highest polarization resistance (927.61 Ω cm^2) was obtained for b-coat and lowest (26.13 Ω cm^2) was observed for si-coat (base silicate electrolyte system) which can be attributed to their morphological characteristics.

3.4. EIS study

The PEO films obtained in electrolyte solutions containing different additives showed different EIS behaviors. The difference was mainly observed in low frequency (LF) range

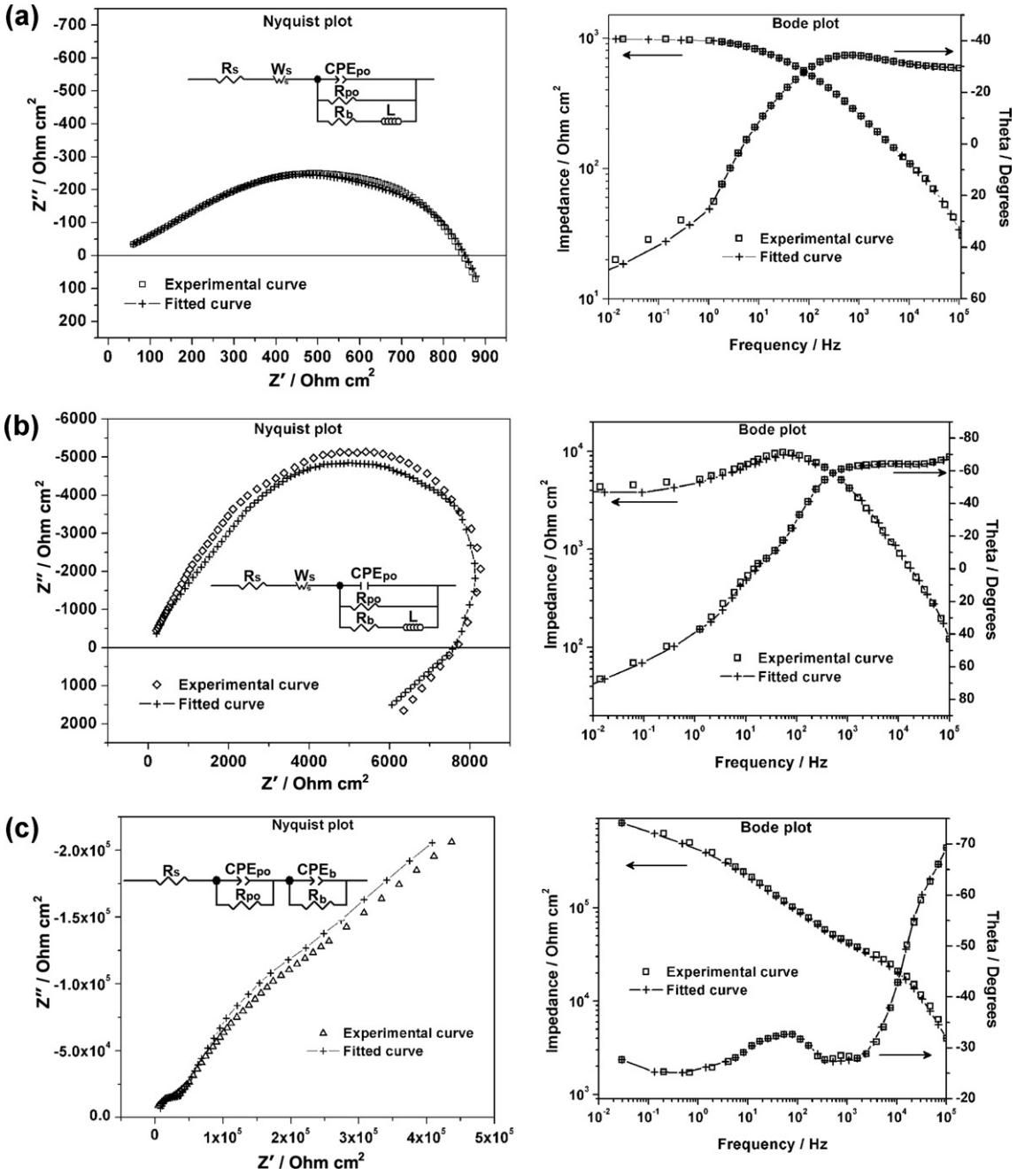

Fig. 5. Nyquist and Bode plots of (a) si-coat, (b) a-coat, (c) b-coat, (d) k-coat, (e) p-coat and (f) u-coat.

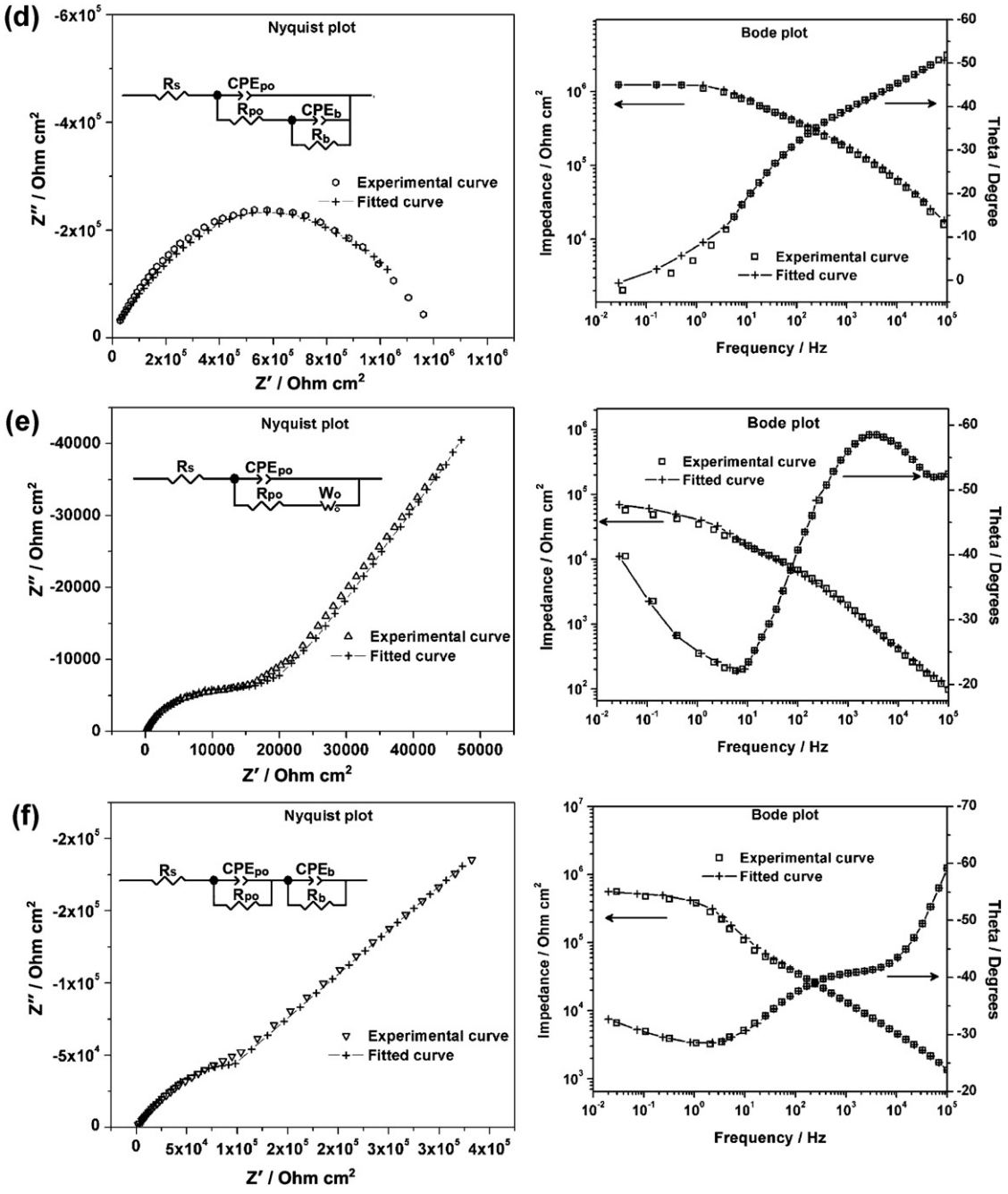

Fig. 5. (*Continued*).

of EIS plots. This is probably because the high frequency (HF) range of impedance diagrams reflects the outer layer properties, while the LF range characterizes the inner layer properties [23]. The Nyquist and Bode plots of experimental and fitted curves of samples treated by PEO in six different electrolyte systems are shown in Fig. 5. The equivalent circuits which best fit the experimental data are shown in the inset of respective Nyquist plots. In all the equivalent circuits, R_s, R_{po} and R_b correspond to solution resistance offered by corrosive electrolyte, pore resistance and inner barrier layer resistance respectively. CPE_{po} and CPE_b represent constant phase elements corresponding to pore and inner barrier layer. CPE is defined as $Z_{CPE} = [C(j\omega)^n]^{-1}$, where $-1 \leq n \leq 1$. The value of n is associated with the non-uniform distribution of current as a result of both the degree of roughness of the surface as well as the degree of the oxide's heterogeneity. W_s and W_o are the finite length Warburg – shot circuit and open circuit terminus respectively whereas L represents the inductance. The impedance results were interpreted using the ZView® software and the equivalent circuits are shown in the inset of Fig. 5(a–f). The fitting quality was evaluated by the chi-squared (χ^2) values, which were of the order of 10^{-4} indicating that the data adjusted well to the proposed equivalent circuit.

3.4.1. si-coat

Fig. 5a shows the Nyquist and Bode plots of experimental and fitting curves of the si-coat. In the HF range, the current is a constant 30° out-of-phase with the potential excitation. The impedance response has then deviated from this relation and at low frequencies it forms an inductive loop below the real axis. Therefore the equivalent circuit contains the elements L and R_b which best fit the experimental data. Analysis of the equivalent circuit shows that the corrosion process was dominated by diffusion control during high frequency perturbations, which is a characteristic of Warburg impedance (W_s). This means that the reactants from the corrosive electrolytes tend to diffuse into the pores of the PEO film. Because of the large pore size in si-coat, as observed from Fig. 2a and Table 2, the diffusion of electrolyte species into the pores will be easier at higher frequencies thereby resulting in adsorption at the inner barrier layer. Due to this adsorption, the Nyquist curve shows an inductive behavior in the LF range. As shown in Table 4, significantly larger values of R_b compared to that of R_{po} suggests that the corrosion protection is provided predominantly by the inner barrier layer. Also, relatively higher value of CPE_{po} (6.1×10^{-5}) reflects the higher double layer capacitance resulting from the high porosity of the coating which is also in good agreement with the pore analysis data (Fig. 2 and Table 2).

3.4.2. a-coat

The Nyquist and Bode plots of experimental and fitting curves for the a-coat is presented in Fig. 5b. Similar to si-coat, Nyquist curve of a-coat also shows diffusion kinetics in the HF range and inductive behavior in LF range. Therefore, the analysis of the equivalent circuit and corresponding mechanism of corrosion process is similar to that of si-coat. However, as compared to si-coat, the values of R_{po} and R_b are higher and CPE_{po} (2.9×10^{-6}) is lower in case of a-coat (Table 4). This suggests that a-coat has higher corrosion resistance and lower surface porosity as compared to si-coat.

3.4.3. b-coat

The Nyquist and Bode plots for the b-coat shown in Fig. 5c demonstrate two time constants which represent the resistance offered by outer porous layer and inner barrier layer, respectively. The high frequency semi-circle demonstrates the outer layer properties whereas the low frequency semi circle demonstrates the inner barrier layer properties. This suggests that the process of corrosion at the outer porous and inner barrier layer is either by diffusion control or charge transfer mechanism. In comparison with the other coatings, b-coat exhibited higher values of both R_{po} and R_b (Table 4) which indicates that the coating has high corrosion resistance. This can be attributed to the comparatively low value of CPE_{po} (1.7×10^{-8}) which in turn indicates that the coating has less porosity. This also conforms to the results obtained by SEM and subsequent pore analysis (Fig. 2 and Table 2).

3.4.4. k-coat

Fig. 5d shows the Nyquist and Bode plots of experimental and fitting curves of the k-coat. The corresponding equivalent

Table 4
EIS data of PEO treated AZ31 Mg alloy in different electrolyte systems.

Sample	CPE_{po}-P	CPE_{po}-T	CPE_b-P	CPE_b-T	$R_{po}/\Omega\,cm^2$	$R_b/\Omega\,cm^2$	L	W_s-P	W_s-T	W_s-R	W_o-P	W_o-T	W_o-R
si-coat	0.46	6.1×10^{-5}	–	–	1.1×10^{2}	1.1×10^{3}	143	0.4	3.2×10^{-2}	8.8×10^{-3}	–	–	–
a-coat	0.92	2.9×10^{-6}	–	–	2.0×10^{2}	3.5×10^{3}	105	0.5	1.5×10^{-3}	2.1×10^{4}	–	–	–
b-coat	0.56	1.7×10^{-8}	0.98	9.5×10^{-10}	7.2×10^{4}	2.1×10^{6}	–	–	–	–	–	–	–
k-coat	0.61	3.9×10^{-8}	0.55	6.8×10^{-8}	3.3×10^{4}	8.9×10^{5}	–	–	–	–	–	–	–
p-coat	0.68	1.3×10^{-6}	–	–	1.7×10^{4}	–	–	–	–	–	0.5	18.8	1.3×10^{5}
u-coat	0.91	3.6×10^{-7}	0.6	6.4×10^{-8}	5.4×10^{4}	1.8×10^{5}	–	–	–	–	–	–	–

circuit shown in the inset of Nyquist plot demonstrates two time constants representing the characteristics of outer porous layer and inner barrier layer. The data of equivalent circuit parameters R_{po} and R_b, listed in Table 4, show that the coating is highly corrosion resistant. However, the resistance values are lesser compared to that of b-coat which can be attributed to the existence of larger sized pores (Fig. 2) as compared to that of b-coat. This can also be confirmed by the higher value of CPE_{po} (3.9×10^{-8}) as compared to b-coat.

3.4.5. p-coat

Fig. 5e shows the Nyquist and bode plots of p-coat and the equivalent circuit which best fits the experimental curve. From the equivalent circuit, it is clear that in the LF range, the corrosion process is mostly diffusion controlled as evidenced by the presence of finite length Warburg element-open circuit terminus (W_o) in series with R_{po}. At low frequencies, in the Nyquist curve, Z'' continued to increase similar to the behavior of a capacitor and terminated in an open circuit and hence W_o is used instead of W_s. This condition arises because at low frequencies the reactants have to diffuse farther, increasing the Warburg impedance. On the other hand, in the high frequency region, Nyquist plot shows a depressed semi circle which can be modeled with parallel double layer capacitance (CPE_{po}) and charge transfer resistance (R_{po}) with a series solution resistance (R_s). This represents the charge transfer kinetics of the corrosion process at high frequencies. Therefore, together with the Warburg impedance, this circuit models a cell where polarization is due to the combination of kinetic and diffusion processes.

3.4.6. u-coat

The experimental data curves of Nyquist, Bode and the corresponding equivalent circuit for u-coat is shown in Fig. 5f. The model used to fit the experimental curves consists of two time constants in series with solution resistance (R_s). Similar to b-coat, the high frequency semi circle represents the porous layer behavior and lower frequency semi circle represents the barrier layer properties. Therefore, the mechanism of corrosion can also be explained similar to that of b-coat. However, the R_{po} and R_b values are lesser than that of both b-coat and k-coat which could be because of the relatively larger pore size as seen from Fig. 2 and Table 2.

In summary, analysis of equivalent circuits of all the above coatings demonstrates a two layered structure of the films as characterized by the presence of two time constants. However, the series and parallel combinations of these time constants are varied. This is because an equivalent circuit is based on a possible physical model which represents the physicochemical process that occurs in the system under investigation. Depending on factors such as film characteristics and whether the charge transfer process is affected by diffusion limitations, the features of EIS spectra and their corresponding equivalent circuits may vary. It can be noted in the present work that each coating exhibits a different phase composition and surface morphology due to the effect of different additives added to the base silicate electrolyte system. This in turn affects the corrosion mechanism of these coatings which is reflected in their respective EIS curves. Thus, different types of equivalent circuits have been modeled to best fit these curves.

From the present study, it can also be observed that there exists a good correlation between the capacitance of each coating and the porosity of its surface. In case of porous electrodes, as the porosity increases, the surface area becomes larger in a given volume, resulting in high capacitance. The same effect is demonstrated in Table 4, which shows that si-coat has a comparatively higher value of CPE_{po} (6.1×10^{-5}), indicating a greater double layer capacitance due to its high porosity. Similarly, lower value of CPE_{po} (1.7×10^{-8}) in case of b-coat reflects its lesser porosity.

Accordingly, from the results of both potentiodynamic polarization tests and EIS study, it is clear that b-coat showed the highest corrosion resistance among all samples. This behavior can be explained by examining the morphology of these samples. As seen from Table 2, although b-coat has a lesser coating thickness (20 μm) compared to other samples, its smaller average pore size (5.6 μm^2) and lower percentage area of porosity (1.1%) are favorable for improving the corrosion resistance. On the other hand, k-coat, which has highest coating thickness of 50 μm, showed lower polarization resistance than b-coat which can be attributed to its higher average size of pore (7.4 μm^2) and percentage area of porosity (2.3%). It is also clear that the si-coat, which has highest values of average pore size and percentage area of porosity showed least corrosion resistance among all the samples. Thus, the pore morphology appears to have a greater effect on the corrosion resistance of PEO treated samples rather than the coating thickness per se.

4. Conclusions

The addition of different additives to the base electrolyte system leads to marked changes in the surface structure, phase composition and electrochemical characteristics of PEO coatings. Using sodium tetra borate as additive to the base electrolyte system was shown to significantly improve the corrosion resistance of the coating by developing a relatively less porous morphology. This coating showed nearly 2×10^6 times higher corrosion resistance than substrate and nearly 35 times higher corrosion resistance compared to the coating formed in base electrolyte system. Further, the role of additives in modifying the corrosion mechanism of coatings developed in different electrolyte systems has been clearly demonstrated by the use of EIS analysis in the present study.

Acknowledgements

The authors would like to acknowledge the facilities procured through the grants received from the Department of Biotechnology, New Delhi (BT/PR-11731/MED/32/99/2008, dated 19-08-2009) and the Department of Science and Technology, New Delhi (SR/FTP/ETA-040/2009, dated 31-12-2009).

References

[1] G. Sundararajan, L.R. Krishna, Mechanisms underlying the formation of thick alumina coatings through the MAO coating technology, Surf. Coat. Technol. 167 (2003) 269–277.

[2] L.O. Snizhko, A.L. Yerokhin, A. Pilkington, N.L. Gurevina, D.O. Misnyankin, A. Leyland, A. Matthews, Anodic processes in plasma electrolytic oxidation of aluminium in alkaline solutions, Electrochim. Acta 49 (2004) 2085–2095.

[3] A.L. Yerokhin, X. Nie, A. Leyland, A. Matthews, Characterisation of oxide films produced by plasma electrolytic oxidation of a Ti–6Al–4V alloy, Surf. Coat. Technol. 130 (2000) 195–206.

[4] E. Matykina, R. Arrabal, P. Skeldon, G.E. Thompson, P. Wang, P. Wood, Plasma electrolytic oxidation of a zirconium alloy under AC conditions, Surf. Coat. Technol. 204 (2010) 2142–2151.

[5] S.V. Gnedenkov, S.L. Sinebryukhov, V.I. Sergienko, Electrochemical impedance simulation of a metal oxide heterostructure/electrolyte interface: a review, Russ. J. Electrochem. 42 (2006) 197–211.

[6] H. Luo, Q. Cai, B. Wei, B. Yu, D. Li, J. He, Z. Liu, Effect of $(NaPO_3)_6$ concentrations on corrosion resistance of plasma electrolytic oxidation coatings formed on AZ91D magnesium alloy, J. Alloys Compd. 464 (2008) 537–543.

[7] L. Shi, Y. Xu, K. Li, Z. Yao, S. Wu, Effect of additives on structure and corrosion resistance of ceramic coatings on Mg–Li alloy by micro-arc oxidation, Curr. Appl. Phys. 10 (2010) 719–723.

[8] A. Bai, Z.J. Chen, Effect of electrolyte additives on anti-corrosion ability of micro-arc oxide coatings formed on magnesium alloy AZ91D, Surf. Coat. Technol. 203 (2009) 1956–1963.

[9] L.R. Krishna, K.R.C. Somaraju, G. Sundararajan, The tribological performance of ultra-hard ceramic composite coatings obtained through microarc oxidation, Surf. Coat. Technol. 163-164 (2003) 484–490.

[10] A. Ghasemi, V.S. Raja, C. Blawert, W. Dietzel, K.U. Kainer, The role of anions in the formation and corrosion resistance of the plasma electrolytic oxidation coatings, Surf. Coat. Technol. 204 (2010) 1469–1478.

[11] J.E. Gray, B. Luan, Protective coatings on magnesium and its alloys – a critical review, J. Alloys Compd. 336 (2002) 88–113.

[12] M.P. Staiger, A.M. Pietak, J. Huadmai, G. Dias, Magnesium its alloys as orthopedic biomaterials: a review, Biomaterials 27 (2006) 1728–1734.

[13] C. Blawert, W. Dietzel, E. Ghali, G. Song, Anodizing treatments for magnesium alloys and their effect on corrosion resistance in various environments, Adv. Eng. Mater. 8 (2006) 511–533.

[14] J. Liang, P.B. Srinivasan, C. Blawert, M. Störmer, W. Dietzel, Electrochemical corrosion behaviour of plasma electrolytic oxidation coatings on AM50 magnesium alloy formed in silicate and phosphate based electrolytes, Electrochim. Acta 54 (2009) 3842–3850.

[15] L.R. Krishna, G. Poshal, G. Sundararajan, Influence of electrolyte chemistry on morphology and corrosion resistance of micro arc oxidation coatings deposited on magnesium, Metall. Mater. Trans. A 41 (2010) 3499–3508.

[16] Q. Cai, L. Wang, B. Wei, Q. Liu, Electrochemical performance of microarc oxidation films formed on AZ91D magnesium alloy in silicate and phosphate electrolytes, Surf. Coat. Technol. 200 (2006) 3727–3733.

[17] C.E. Barchiche, E. Rocca, C. Juers, J. Hazan, J. Steinmetz, Corrosion resistance of plasma-anodized AZ91D magnesium alloy by electrochemical methods, Electrochim. Acta 53 (2007) 417–425.

[18] R. Arrabal, E. Matykina, P. Skeldon, G.E. Thompson, A. Pardo, Transport of species during plasma electrolytic oxidation of WE43-T6 magnesium alloy, J. Electrochem. Soc. 155 (2008) C101–C111.

[19] L.S. Wang, C.X. Pan, Characterisation of microdischarge evolution and coating morphology transition in plasma electrolytic oxidation of magnesium alloy, Surf. Eng. 23 (2007) 324–328.

[20] S. Ono, H. Kijima, N. Masuko, Microstructure and voltage–current characteristics of anodic films formed on magnesium in electrolytes containing fluoride, Mater. Trans. 44 (2003) 539–545.

[21] H.F. Guo, M.Z. An, Growth of ceramic coatings on AZ91D magnesium alloys by micro-arc oxidation in aluminate–fluoride solutions and evaluation of corrosion resistance, Appl. Surf. Sci. 246 (2005) 229–238.

[22] M. Stern, A.L. Geary, Electrochemical polarization. I. A theoretical analysis of the shape of polarization curves, J. Electrochem. Soc. 104 (1957) 56–63.

[23] H. Duan, C. Yan, F. Wang, Effect of electrolyte additives on performance of plasma electrolytic oxidation films formed on magnesium alloy AZ91D, Electrochim. Acta 52 (2007) 3785–3793.